Interaction of Lyapunov vectors in the formulation of the nonlinear extension of the Kalman filter

Luigi Palatella[1,*] and Anna Trevisan[2]

[1]*Istituto di Scienze dell'Atmosfera e del Clima ISAC–CNR, UOS di Lecce, Str. Prov. Lecce-Monteroni km 1,200, I-73100 Lecce, Italy; INFN sede di Lecce*

[2]*Istituto di Scienze dell'Atmosfera e del Clima ISAC–CNR, via Gobetti 101, I-40129 Bologna, Italy*

(Received 4 December 2014; published 9 April 2015)

When applied to strongly nonlinear chaotic dynamics the extended Kalman filter (EKF) is prone to divergence due to the difficulty of correctly forecasting the forecast error probability density function. In operational forecasting applications ensemble Kalman filters circumvent this problem with empirical procedures such as covariance inflation. This paper presents an extension of the EKF that includes nonlinear terms in the evolution of the forecast error estimate. This is achieved starting from a particular square-root implementation of the EKF with assimilation confined in the unstable subspace (EKF-AUS), that is, the span of the Lyapunov vectors with non-negative exponents. When the error evolution is nonlinear, the space where it is confined is no more restricted to the unstable and neutral subspace causing filter divergence. The algorithm presented here, denominated EKF-AUS-NL, includes the nonlinear terms in the error dynamics: These result from the nonlinear interaction among the leading Lyapunov vectors and account for all directions where the error growth may take place. Numerical results show that with the nonlinear terms included, filter divergence can be avoided. We test the algorithm on the Lorenz96 model, showing very promising results.

DOI: 10.1103/PhysRevE.91.042905 PACS number(s): 05.45.Gg, 05.45.Pq

I. INTRODUCTION

State estimation is a classical problem in control theory: The Kalman filter estimates the state of a system by combining forecasts with incoming observations in a sequential way and it is optimal in the sense of minimizing the error variance when the system dynamics and the observation operator are linear. The extended Kalman filter (EKF) [1] is the extension of the linear results to the nonlinear case and is based on the tangent linear evolution of the errors.

The range of applications of the Kalman filter and EKF is enormous and involves researchers coming from very different scientific communities. Without any claim of completeness, the most common applications relate to navigation and control (GPS, localization, target tracking) [2], geophysical systems [3,4], pattern recognition [5,6], electrochemical systems dynamics [7,8], biomedical signal processing [9], manufacturing processes [10], and many others. For a comprehensive review including also techniques alternative to the Kalman filter see Refs. [11,12].

When the dynamics is nonlinear but the error distribution is Gaussian the EKF can capture the linear evolution of the error by evolving and updating its covariance: Under the hypothesis of linearity and Gaussianity of the error the EKF provides the optimal solution. However, even small nonlinearities that unavoidably occur when the observations are not sufficiently dense and accurate can cause filter divergence; this is because the error covariance and its linear evolution prescribed by the EKF equations is no more adequate to describe the characteristics of the real error distribution.

One way in which this discrepancy can manifest itself is the following. The real error cannot be controlled by the EKF because it is not confined in the subspace spanned by the estimated covariance; in other words, the EKF error covariance is rank deficient. In fact, Palatella and Trevisan [13] have shown that the rank of error covariance of the full EKF converges to the number of positive and neutral Lyapunov exponents as a consequence of the linearity assumption. It then follows that the EKF and a square-root [14] implementation that restricts the assimilation to the unstable subspace (EKF-AUS) lead to the same solution. For the original introduction of the AUS we refer the reader to Refs. [15–19].

In synthesis, let n be the phase-space dimension and m the number of unstable and neutral directions. By restricting the assimilation of observations to the unstable and neutral directions of the nonlinear estimated trajectory, EKF-AUS only needs m perturbations and $n \times m$ covariance matrices instead of the full $n \times n$ EKF matrices. This can be useful in many applications. In fact, when the dimension of the unstable and neutral subspace is significantly smaller than the total number of degrees of freedom, the problem becomes computationally tractable even for very high dimensional systems [15].

Building upon these results, this paper presents an algorithm that accounts for nonlinearities in the error evolution by taking into account higher-order terms in the expansion and expressing them in terms of interactions among the Lyapunov directions. This algorithm is referred to as EKF-AUS-NL. In the case of quadratic nonlinearities in the equations of motions the nonlinear terms in the error evolution are perfectly described. The algorithm is demonstrated in the Lorenz96 [20] model to show that it is possible to avoid filter divergence in a wide range of observation errors and time intervals between observations when the EKF fails to do so.

Extensive use of the EKF in many fields of application that appears in the literature indicates that it works well when the instability and nonlinearity are not too strong [11]. The formulation of the EKF in terms of covariances, second-order moments of the error PDF, is obtained by linearizing the dynamics. The authors of Ref. [21] introduced higher-order terms in an extension of the EKF that includes third- and fourth-order moments.

*luigi.palatella@yahoo.it

 ©2015 American Physical Society

In geophysical literature ensemble Kalman filters (EnKF) are very popular algorithms [22–25] that can be applied to models with a very large number of degrees of freedom; they are based on a Monte Carlo approach aimed to deal with non-Gaussianity and nonlinearity of the error distribution. They use the full nonlinear model to propagate the members forward in time, but no matter how these spread in phase space, the Gaussian approximation is kept in the analysis update. However, with a notable exception [26], various empirical strategies often need to be introduced in EnKFs, such as covariance localization and multiplicative and/or additive covariance inflation [23–25].

The minimum number of ensemble members necessary to control the EnKF error was found [27] to be in agreement with the theoretical result by Trevisan and Palatella for the EKF [13]. When the error dynamics is linear, the minimum number of perturbations is equal to the number of unstable and neutral directions: Nonlinearity can only increase the number of possible directions of error growth. The same result was obtained in the context of four-dimensional (4D) variational assimilation by Trevisan *et al.*, who introduced 4DVar with assimilation in the unstable subspace (4DVar-AUS) [28]; this algorithm uses a number of perturbations that are linearly evolved and converge to the Lyapunov vectors with positive and neutral exponents along the assimilation cycle. This number of perturbations, used in place of the adjoint model in the 4DVar-AUS algorithm [29,30], is sufficient to produce an analysis error that is smaller than that of the full 4DVar. For the same reasons discussed for the EKF, also in the case of 4DVar-AUS, when nonlinearity becomes important it is necessary to increase the number of perturbations in order to increase the dimension of the subspace where the assimilation is confined.

In this paper we introduce the formalism that extends the EKF-AUS to account for nonlinearity; to this end we introduce second-order derivatives in the perturbative equations and quadratic interactions among Lyapunov vectors. The outline of the paper is the following: In Sec. II we briefly review the EKF and EKF-AUS algorithm, and then we present the new EKF-AUS-NL algorithm in Sec. III. In Sec. IV we demonstrate its performance on the Lorenz96 model [20]. We investigate how, with the introduction of nonlinear terms in a range of parameter values that causes failure of the EKF, one can avoid filter divergence in the Lorenz96 model. We also show the geometrical interpretation of our approach with an example of analysis-forecast cycle on the Lorenz63 model [31]. Finally, the conclusions follow in Sec. V.

II. THE BACKGROUND: EKF AND EKF-AUS

The EKF-AUS filter is a particular square-root implementation [14] of the EKF and was formally presented in Ref. [13]. Here we briefly summarize how it works. Given a dynamical system driven by the differential equation

$$\frac{d\mathbf{x}}{dt} = F(\mathbf{x}), \tag{1}$$

where $\mathbf{x}$ is an n-dimensional vector, the assimilation experiment is set up by performing the time evolution between the times t_{k-1} and t_k (not necessarily equally spaced) of two trajectories according to Eq. (1). One trajectory, the solution of Eq. (1), is identified as the truth, while the other is obtained as a sequence of analysis states. The truth is used to build up an artificial p-dimensional measurement at time t_k given by

$$y_j^o = \mathcal{H}_j(\mathbf{x}_k) + \sigma_o \eta_j, \quad j \in [1,p], \tag{2}$$

where $\mathcal{H}()$ is the observation operator and η_j are Gaussian uncorrelated variables with zero mean and unitary variance. σ_o is the observation error standard deviation. The analysis is performed at observation times, based on observations and the forecast $\mathbf{x}_k^f$ that starts from analysis state.

The EKF equations that are used to construct the sequence of analysis states are

$$\begin{aligned} &\text{forecast: } \mathbf{x}_k^f = \mathcal{M}\left(\mathbf{x}_{k-1}^a\right), \\ &\text{analysis: } \mathbf{x}_k^a = \mathbf{x}_k^f - \mathbf{K}_k \mathcal{H}\left(\mathbf{x}_k^f\right) + \mathbf{K}_k \mathbf{y}_k^o, \end{aligned} \tag{3}$$

for the trajectory, while the error covariance matrices obey

$$\begin{aligned} &\text{forecast: } \mathbf{P}_k^f = \mathbf{M}_k \mathbf{P}_{k-1}^a \mathbf{M}_k^T, \\ &\text{analysis: } \mathbf{P}_k^a = (\mathbf{I} - \mathbf{K}_k \mathbf{H}) \mathbf{P}_k^f, \end{aligned} \tag{4}$$

where $\mathcal{M}$ is the nonlinear evolution operator solving Eq. (1), $\mathbf{M}$ is the Jacobian of $\mathcal{M}$, $\mathbf{K}_k$ is the *gain matrix*

$$\mathbf{K}_k = \mathbf{P}_k^f \mathbf{H}^T \left(\mathbf{H} \mathbf{P}_k^f \mathbf{H}^T + \mathbf{R}\right)^{-1}, \tag{5}$$

and $\mathbf{H}$ is the Jacobian of the observation operator $\mathcal{H}$. In the present formulation, we assumed that the evolution equations given by Eq. (1) are known, an approach referred to as the "perfect model scenario."

If the dynamical system of Eq. (1) is chaotic, then its tangent space can be divided into stable, neutral, and unstable manifolds of dimension given by the numbers N^+, N^0, and N^- of positive, null, and negative Lyapunov exponents, respectively ($N^+ + N^0 + N^- = n$).

The EKF-AUS algorithm is obtained by performing the assimilation in a manifold of dimension m. When m is equal to the number n of degrees of freedom of the system, the algorithm solves the standard EKF equations. When $m = N^+ + N^0$, the reduced form, with assimilation in the unstable subspace (EKF-AUS) is obtained. In the following we omit the time index k for clarity.

The analysis error covariance matrix is expressed as

$$\mathbf{P}^a = \mathbf{X}_a \mathbf{X}_a^T, \tag{6}$$

with $\mathbf{X}_a$ a square root of $\mathbf{P}^a$ defined below in Eq. (14).

We then have that during the forecast step the time evolution acts on the columns of $\mathbf{P}^a$ (the *perturbations*) as

$$\mathbf{P}^f = \mathbf{M}\mathbf{X}_a(\mathbf{M}\mathbf{X}_a)^T = \mathbf{X}_f \mathbf{X}_f^T. \tag{7}$$

After the time evolution, we orthonormalize the perturbations $\delta\mathbf{x}_i^f$, i.e., the columns of $\mathbf{X}^f$, obtaining

$$\begin{aligned} &\delta\mathbf{x}_i^f \to \mathbf{e}_i^f \text{ Graham} - \text{Schmidt algorithm} \\ &\mathbf{X}_f = \left[\delta\mathbf{x}_1^f, \delta\mathbf{x}_2^f, \ldots, \delta\mathbf{x}_m^f\right], \quad \mathbf{E}_f = \left[\mathbf{e}_1^f, \mathbf{e}_2^f, \ldots, \mathbf{e}_m^f\right]. \end{aligned} \tag{8}$$

We cast the forecast error covariance matrix in the form

$$\mathbf{P}^f = \mathbf{X}_f \mathbf{X}_f^T = \mathbf{E}_f \mathbf{E}_f^T \mathbf{X}_f \mathbf{X}_f^T \mathbf{E}_f \mathbf{E}_f^T = \mathbf{E}_f \Gamma_f \mathbf{E}_f^T, \tag{9}$$

where $\Gamma_f = \mathbf{E}_f^T \mathbf{X}_f \mathbf{X}_f^T \mathbf{E}_f$ and noting that $\mathbf{E}_f \mathbf{E}_f^T$ is the identity matrix in the subspace spanned by $\mathbf{e}_i^f$.

The analysis step is given by

$$\begin{aligned} \mathbf{x}^a &= \mathbf{x}^f + \mathbf{K}[\mathbf{y}^o - \mathcal{H}(\mathbf{x}^f)] \\ \mathbf{K} &= \mathbf{E}_f \Gamma_f \mathbf{E}_f^T \mathbf{H}^T \left(\mathbf{H}\mathbf{E}_f \Gamma_f \mathbf{E}_f^T \mathbf{H}^T + \mathbf{R}\right)^{-1} \\ \mathbf{P}^a &\equiv \mathbf{E}_f \Gamma_a^{'} \mathbf{E}_f^T = (\mathbf{I} - \mathbf{K}\mathbf{H}) \mathbf{E}_f \Gamma_f \mathbf{E}_f^T, \end{aligned} \tag{10}$$

collecting $\mathbf{E}_f$ and $\mathbf{E}_f^T$ from the left and the right in the third of Eq. (10), after substituting the expression for $\mathbf{K}$, we obtain

$$\Gamma_a^{'} = \Gamma_f - \Gamma_f \mathbf{E}_f^T \mathbf{H}^T \left(\mathbf{R} + \mathbf{H}\mathbf{E}_f \Gamma_f \mathbf{E}_f^T \mathbf{H}^T\right)^{-1} \mathbf{H}\mathbf{E}_f \Gamma_f \tag{11}$$

and

$$\mathbf{P}^a \equiv \mathbf{E}_f \Gamma_a^{'} \mathbf{E}_f^T = \mathbf{E}_f \mathbf{U} \Gamma_a \mathbf{U}^T \mathbf{E}_f^T, \tag{12}$$

where $\mathbf{U}$ is orthogonal and diagonalizes $\Gamma_a^{'}$ in $\Gamma_a = \mathrm{diag}[\gamma_i^2]$. A new set of orthonormal vectors $\mathbf{E}_a$ is obtained

$$\mathbf{E}_a = \mathbf{E}_f \mathbf{U} = \left[\mathbf{e}_1^a, \mathbf{e}_1^a, \ldots, \mathbf{e}_m^a\right]. \tag{13}$$

Thus we have

$$\mathbf{P}^a = \mathbf{E}_a \Gamma_a \mathbf{E}_a^T = \mathbf{X}_a \mathbf{X}_a^T = \textstyle\sum_{i=1}^m \delta\mathbf{x}_i \delta\mathbf{x}_i^T, \tag{14}$$

with $\mathbf{X}_a = [\delta\mathbf{x}_1^a, \delta\mathbf{x}_2^a, \ldots, \delta\mathbf{x}_m^a] = [\gamma_i \mathbf{e}_1^a, \gamma_i \mathbf{e}_2^a, \ldots, \gamma_i \mathbf{e}_m^a]$. The vectors $\delta\mathbf{x}_i^a$, columns of $\mathbf{X}_a$, are the new (orthogonal) perturbations. Using the analogy with the algorithm of Ref. [32], the authors of Ref. [13] showed that, asymptotically, $\delta\mathbf{x}_i^a$ and $\delta\mathbf{x}_i^f$ span the same subspace as the leading $(N^+ + N^0)$ Lyapunov vectors because errors in the stable subspace decay along the assimilation cycle so only errors in the unstable and neutral subspace survive the filtering process.

As a consequence, the rank of the EKF covariance matrix, initially equal to the total number of degrees of freedom of the system, asymptotically reduces to the dimension of the unstable and neutral subspace. Therefore, the EKF equations and the reduced form of the algorithm, EKF-AUS, provide the same solution.

These results hold when observations are sufficiently dense and accurate that error dynamics is linear, a necessary condition for the EKF to work properly without being subject to divergence episodes.

III. THE NONLINEAR EXTENSION OF EKF-AUS: THE EKF-AUS-NL ALGORITHM

We are now ready to show how to include the nonlinear behavior of error evolution during the forecast step in the framework of EKF-AUS. The nonlinear term may have two effects. It can change the magnitude of the m vectors, altering the size of the error in the space spanned by the linear error perturbations. In addition, it can also induce the presence of error in directions that are outside the unstable and neutral subspace. This second effect is surely more important. Indeed, the mere change of magnitude of the linear error is typically associated to a worsening of the filter performance but not necessarily to its divergence. The worst case is when nonlinearity introduces additional directions where errors may grow; if this happens the filter is almost always prone to divergence. This is because the estimated analysis error in these directions is zero and the filter is not able to correct it; recall that, due to the linear assumption Eq. (7), the rank of the error covariance matrix is reduced to the numbers of non-negative Lyapunov exponents also in the EKF [13].

The nonlinear evolution of the actual error $\Delta \equiv \mathbf{x}(t) - \mathbf{x}^{\mathbf{t}}(t)$ in the interval between the analysis time $t = 0$ and the forecast time $t = \tau$ is

$$\begin{aligned} \frac{d}{dt}\Delta_i &= F_i(\mathbf{x}^a) - F_i(\mathbf{x}^{\mathbf{t}}) \\ &= \frac{\partial F_i}{\partial x_j}\Delta_j + \frac{1}{2}\frac{\partial F_i}{\partial x_j \partial x_k}\Delta_j \Delta_k + O(\Delta^3), \end{aligned} \tag{15}$$

where

$$\mathbf{x}(0) = \mathbf{x}^a, \quad \mathbf{x}(\tau) = \mathbf{x}^f. \tag{16}$$

Consequently, $\Delta(0)$ is the actual analysis error, while $\Delta(\tau)$ is the actual forecast error. Where not specified we use the Einstein's convention on summation for repeated indexes. The Taylor expansion can be calculated at $\mathbf{x}^a$ obtaining

$$\begin{aligned} \frac{d}{dt}(\mathbf{x}^{\mathbf{t}} - \mathbf{x}^a)_i &= F_{i,j}|_{\mathbf{x}=\mathbf{x}^a}(\mathbf{x}^{\mathbf{t}} - \mathbf{x}^a) \\ &\quad + \frac{1}{2}F_{i;jk}(\mathbf{x}^{\mathbf{t}} - \mathbf{x}^a)_j(\mathbf{x}^{\mathbf{t}} - \mathbf{x}^a)_k, \end{aligned} \tag{17}$$

where we use the notation

$$F_{i,j} \equiv \frac{\partial F_i(\mathbf{x})}{\partial x_j}, \quad F_{i;jk} \equiv \frac{\partial^2 F_i(\mathbf{x})}{\partial x_j \partial x_k}. \tag{18}$$

Remembering the definition of Δ we have

$$\frac{d}{dt}\Delta_i(t) = F_{i,j}x|_{\mathbf{x}=\mathbf{x}^a}\Delta_j(t) - \frac{1}{2}F_{i;jk}\Delta_j(t)\Delta_k(t). \tag{19}$$

When the second order is the highest nonlinearity, as typical in many geophysical applications where advection is the only nonlinear term, this equation for the time evolution of the error $\Delta(t)$ is exact. For this reason we drop the argument $\mathbf{x}$ in the second-order derivative, because in the case of second-order nonlinearity this term becomes constant. The first term in Eq. (19) is nothing but the tangent linear evolution of the error and $\mathbf{M}$ is the linear operator that solves this differential equation without the nonlinear term. The second term is the term involving nonlinearities.

Following the notation of Ref. [13], let us write the actual analysis error $\Delta(0)$ as

$$\Delta_i(0) = \sum_{s=1}^m \alpha_s \mathbf{X}_{is}^a, \tag{20}$$

i.e., as a linear combination of the columns of the matrix $\mathbf{X}^a$, as shown in Sec. II. The coefficients α_s are unknown because we obviously do not know the actual error. Indeed Eq. (20) can be intended as a definition of α_s.

We can separate the time derivative of the error in a linear and in a nonlinear part, namely (Einstein notation except for $r,s \in [1,m]$)

$$\frac{d}{dt}\Delta_i(t) = F_{i,j}\sum_{s=1}^m \alpha_s \mathbf{X}_{js}^a + \frac{1}{2}F_{i;jk}\sum_{s=1}^m \alpha_s \mathbf{X}_{js}^a \sum_{r=1}^m \alpha_r \mathbf{X}_{kr}^a. \tag{21}$$

We then have for the actual error at forecast time τ,

$$\Delta(\tau) = \Delta(0) + \int_0^\tau dt \left[F_{i,j} \sum_{s=1}^{m} \alpha_s \mathbf{X}^a_{js} + \frac{1}{2} F_{i;jk} \sum_{s=1}^{m} \alpha_s \mathbf{X}^a_{js} \sum_{r=1}^{m} \alpha_r \mathbf{X}^a_{kr} \right]. \quad (22)$$

The actual forecast error is unknown but our goal is to calculate the forecast error covariance matrix that can be expressed as

$$\begin{aligned} \mathbf{P}^f_{ij} &= \langle \Delta_i(\tau) \Delta_j(\tau) \rangle \\ &= \langle \mathcal{L}_i \mathcal{L}_j \rangle + \langle \mathcal{N}_i \mathcal{N}_j \rangle + \langle \mathcal{N}_i \mathcal{L}_j \rangle + \langle \mathcal{L}_i \mathcal{N}_j \rangle, \end{aligned} \quad (23)$$

where the vectors $\mathcal{L}$,$\mathcal{N}$ are given by

$$\begin{aligned} \mathcal{L}_i &= \Delta_i(0) + \int_0^\tau dt\, F_{i,j} \sum_{s=1}^{m} \alpha_s \mathbf{X}^a_{js} \\ \mathcal{N}_i &= \int_0^\tau dt \frac{1}{2} F_{i;jk} \sum_{s=1}^{m} \alpha_s \mathbf{X}^a_{js} \sum_{r=1}^{m} \alpha_r \mathbf{X}^a_{kr}. \end{aligned} \quad (24)$$

The brackets $\langle\rangle$ represent a statistical average that can be computed if the distributions of α_j, with $j \in [1,m]$, are known. The calculation of the different terms of Eq. (23) uses the hypothesis that the actual analysis error is Gaussian with covariance given by $\mathbf{P}^a$. If the filter is working well, we then have that the direction and the magnitude of the vectors given by $\mathbf{X}^a$ are a good representation of the actual analysis error. This means that the unknown coefficient α_j, under these hypotheses, are Gaussian distributed with zero mean and unitary variance. The detailed calculation of the different terms is shown in Appendix A. After the steps described in Appendix A, we obtain that the error "perturbations" (columns of) $\mathbf{X}$ evolve from $\mathbf{X}^a$ at $t = 0$ to $\mathbf{X}^f$ at $t = \tau$ according to the differential equation

$$\begin{aligned} \frac{d}{dt}\mathbf{X}_{is} &= F_{i,j}\mathbf{X}_{js}, \quad s \leqslant m \\ \frac{d}{dt}\mathbf{X}_{is(q,r)} &= F_{i,j}\mathbf{X}_{js(q,r)} + \frac{1}{2}\bar{\alpha} F_{i;jk}\mathbf{X}_{jq}\mathbf{X}_{kr}, \\ q \leqslant r;\ q,r \in [1,m_l]; &\quad s(q,r) = m + \sum_{r=1}^{m_l}\sum_{q=1}^{q\leqslant r} 1, \end{aligned} \quad (25)$$

where m_l is the number of linear vectors that we involve in the nonlinear interactions. One may of course consider all the possible nonlinear interactions of the m perturbation vectors. This leads to other $m(m+1)/2$ vectors to be handled. In several instances this approach cannot be followed because the number of vectors to be considered becomes much too large. For this reason we may limit the nonlinear interactions to the leading (most unstable) m_l vectors. The condition on the indexes s,m_l,t is nothing but a convention to keep the vectors evolving according to the nonlinear terms separated from the first $m = N^+ + N^0$ vectors already involved in the EKF-AUS algorithm.

As discussed in Appendix A, the analytical calculations lead to a slightly different form of the equations driving the evolution of $\mathbf{X}^a$. The main difference is the choice to let each nonlinear interaction drive a single perturbation vector, while in the exact calculations the interaction of each vector with itself is summed up in a single term. The calculations lead to different prefactors in front of the self-interactions (of the kind $F_{i;jk}X_{jq}X_{kq}$ with prefactor $\sqrt{3}$) with respect to cross-interaction terms (like $F_{i;jk}X_{jq}X_{kr}$ with $q \neq r$, giving $\sqrt{2}$). The exact prefactors are deeply based on the Gaussian assumption on the analysis error at time $t = 0$. For this reason we decide to use a common prefactor $\bar{\alpha} = \sqrt{3}$ for all the terms. We performed some tests with different values of $\bar{\alpha}$ without substantial changes in the results. In any case these numerical factors can be tuned according to the need of higher precision (smaller $\bar{\alpha}$) or to avoid filter divergence (larger $\bar{\alpha}$).

We point out again that the main, and slightly more subtle, effect of the nonlinear terms is to distort the ellipsoid error and increase the dimension of the space in which the error spans. This effect is due both to nonlinear interaction of each column of $\mathbf{X}^a_s$ with itself and to interaction between different columns. This aspect is important because in ensemble approaches to the Kalman filter, one could argue that the nonlinear terms are considered by evolving the full model and studying the departure of different ensemble members. This effect corresponds only to the self-interaction terms (like $F_{i;jk}X_{jq}X_{kq}$) while the cross-interaction terms like $F_{i;jk}X_{jq}X_{kr}$ are generally not considered in a standard ensemble approach. In Appendix B we show how to take into account cross terms when we are not given the tangent linear and second-order derivative of Eq. (1).

In summary, in EKF-AUS-NL, we evolve the vectors $\mathbf{X}^a$ to $\mathbf{X}^f$ according to Eq. (25), used in place of Eq. (7). Then we follow the same steps of the EKF-AUS algorithm. Namely we orthonormalize the columns of $\mathbf{X}^f$ as in Eq. (8) and then we reconstruct $\mathbf{P}^f$ by computing Γ^f Eq. (9).

Indeed, we stress that in the analysis step the algorithm we are proposing is still the linear EKF-AUS algorithm. We still use a forecast error covariance $\mathbf{P}^f$ as if the distribution were Gaussian, but this time the error has nonzero components also in the directions generated by the nonlinear terms of Eq. (25). This means that, from a geometrical point of view, we circumscribe the actual error distribution that can be quite peculiar and strongly non-Gaussian (see, for example, Fig. 1) with an ellipsoid with augmented dimension due to the nonlinear terms. To achieve this goal the best way is to maintain separated the linear error vectors and the other vectors generated by the nonlinear terms of Eq. (25).

IV. RESULTS

For an illustration of the effect of increasing the dimension of the space spanned by the forecast error due to nonlinearities we first show an example of application to the Lorenz63 model.

A. An illustrative example in the Lorenz63 model

The model is the standard Lorenz63 model [31] given by

$$\begin{aligned} \frac{dx}{dt} &= \sigma(y - x) \\ \frac{dy}{dt} &= rx - y - xz \\ \frac{dz}{dt} &= xy - bx \end{aligned} \quad (26)$$

with, as usual, $\sigma = 10, r = 28, b = 8/3$.

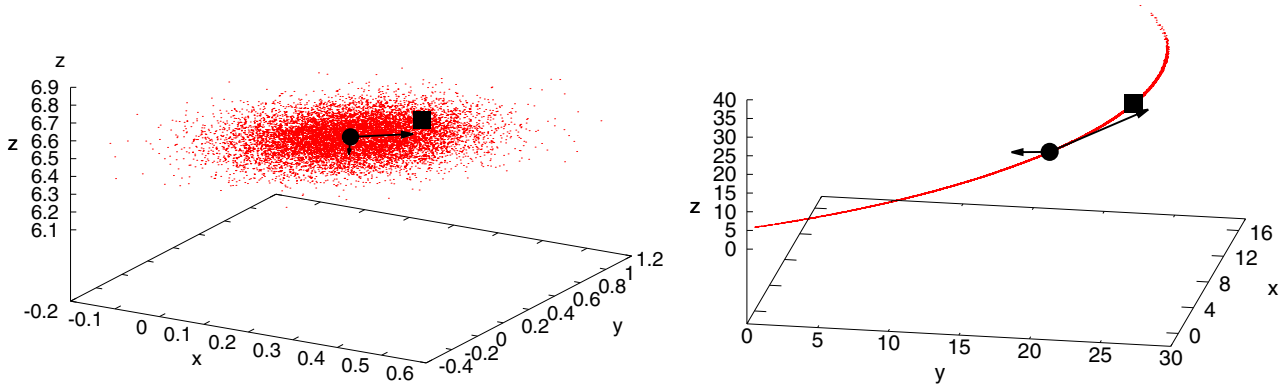

FIG. 1. (Color online) Left panel: The black filled circle denotes the analysis. The black filled square denotes the truth. The two orthogonal black solid vectors starting from the analysis are the two leading error vectors after the analysis (the two first columns of $\mathbf{X}_a$: $\delta\mathbf{x}_1^a$,$\delta\mathbf{x}_2^a$). The third column (i.e., the nonlinear vector) is not visible, as its magnitude is very small. The clouds of red dots are 10 000 ensemble copies of the analysis distributed according to the analysis error. Right panel: The black filled circle is the forecast, i.e., the time evolution of the analysis (same symbol) of the left panel. The black filled square is the time evolution of the truth, so it is the truth at this time. The black solid vector pointing to the right is the first column of the forecast error matrix, namely the evolution of $\delta\mathbf{x}_1^a$. The evolution of $\delta\mathbf{x}_2^a$ is very small and cannot be seen. The black solid vector pointing to the left is the cumulative nonlinear vector. The red dots (distributed along a sort of parabola) are the time evolution of the clouds of red dots of the left panel and represent a sampling of the forecast error distribution.

We perform a data assimilation experiment in the perfect model scenario with a truth trajectory used to construct the observations. The observation operator $\mathcal{H}$ is the identity (we measure all three variables) and the measurement error σ_o is supposed to be Gaussian. The number of neutral and unstable vectors in this case is $m = 2$. The number of possible nonlinear terms is, consequently, $m(m+1)/2 = 3$. As the total number of dimensions is 3 in this case we are forced to sum together all the nonlinear terms of Eq. (25) to obtain a single cumulative nonlinear vector.

In order to illustrate how the algorithm operates, we choose, along the assimilation cycle, a condition in which, without the nonlinear terms, filter divergence occurred. In particular, we use $\sigma_o = 0.2$ and the time interval between analysis and forecast $\tau = 0.375$. Looking for an analysis-forecast interval in which the nonlinear term becomes relevant in magnitude, we selected the condition shown in Fig. 1.

In the left panel, we show the analysis step: The black filled circle indicates the analysis and the black filled square the truth. The two orthogonal solid black vectors starting from the analysis are the two leading perturbation vectors after the analysis (the first two columns of $\mathbf{X}_a$: $\delta\mathbf{x}_1^a$,$\delta\mathbf{x}_2^a$). The third column (i.e., the cumulative nonlinear vector) is not visible, as its magnitude is very small. The cloud of red dots are obtained adding to the analysis $\mathbf{x}^a$ a linear combination $\alpha_1\delta\mathbf{x}_1^a + \alpha_2\delta\mathbf{x}_2^a$, where $\alpha_{1,2}$ are Gaussian random numbers with zero mean and unitary variance. The cloud so represents the "ellipsoid" of the analysis error. As shown the truth is inside this ellipsoid. This means that nothing "pathological" can be diagnosed at this moment.

In the right panel we show the forecast step obtained after a time integration interval τ. The black filled circle is the forecast, the time evolved from the analysis (same symbol) of the left panel. The black filled square is evolved from the truth so it is the truth at this time. The black solid vector pointing to the right is obtained by linearly evolving $\delta\mathbf{x}_1^a$, the leading Lyapunov vector. The vector obtained by evolving $\delta\mathbf{x}_2^a$ is very small and cannot be seen. The black vector pointing to the left is the cumulative nonlinear vector. The red dots result from the time evolution of the cloud of red dots of the left panel. The ellipsoid has evolved, due to nonlinearity, into a sort of parabola, the "line" of red dots in the 3D space and the truth is on this line.

This means that the linear error vectors (the one pointing to the right tangent to the parabola and the other that is negligibly small) cannot account for the error component outside the forecast ellipsoid. Only with the help of the cumulative nonlinear vector that points toward the focus of the parabola can the filter take into account the actual error and correct it in the analysis step.

In practice, the algorithm uses, with the aid of the cumulative nonlinear vector, a corrected ellipsoid, containing the parabola composed by the red dots, representing the forecast error covariance. This means that for what concerns the analysis step the technique is still based on a Gaussian distribution but we use a Gaussian forecast error distribution that includes the nonlinear directions obtained from the error evolution and thus "contains" the actual forecast error.

In synthesis an accurate description of the directions that captures the distribution where the truth lies is obtained with just two vectors, the leading Lyapunov vector and the cumulative nonlinear vector. With an ensemble approach, a very large number of ensemble members would be necessary in order to obtain an equivalent description of the distribution.

B. An evaluation of the algorithm on the Lorenz96 model

The divergence of a data assimilation algorithm can be considered a stochastic property since it may be due to a combination of large measurement errors (an intrinsic stochastic property) and particularly unstable conditions. This suggests that a correct way to evaluate the capability of an algorithm to avoid divergence due to nonlinearity in the error dynamics is to estimate the mean divergence time. We will

TABLE I. The index arrangement for the Lorenz96 test with $m = 14$, $n = 40$, $m_l = 4$.

s	15	16	17	18	19	20	21	22	23	24
r	1	2	2	3	3	3	4	4	4	4
q	1	1	2	1	2	3	1	2	3	4

compare the divergence times of the nonlinear algorithm with those of its linear counterpart in the Lorenz96 model [20].

The governing equations are

$$\frac{d}{dt}x_j = (x_{j+1} - x_{j-2})x_{j-1} - x_j + F \tag{27}$$

with $j = 1,\ldots,n$. The variables x_j represent the values of a scalar meteorological quantity at n equally spaced geographic sites on a periodic longitudinal domain. The model has chaotic behavior for the value of the forcing, $F = 8$, used in most studies, and with the value of n used in this paper. The number of variables n of the model is varied to obtain different systems with a different number of degrees of freedom and, consequently, a different number of positive Lyapunov exponents. With $n = 40,60,80$ the systems have 13,19,25 positive Lyapunov exponents, respectively. In this paper we test the algorithm using $n = 40$ and, consequently, $m = N^+ + N^0 = 14$.

Obviously, if the number of linear perturbation is m, then the number of new vectors is $m(m+1)/2$, which, in the present case, exceeds the total dimension of the state vector n. A reasonable approach is to select only the m_l first (i.e., the largest) linear vectors and compute the nonlinear terms using only these vectors. We set $m_l = 4$, thus obtaining 10 extra vectors in addition to the 14 orthogonalized Lyapunov vectors of the 40-variables model. In our case this means that we use a total of 24 perturbations. The indexes of the nonlinear vectors thus become those shown in Table I.

We consider a time interval between assimilation steps $\tau = 4,5,6,7,8,10,12,14,16 \times dt$ with $dt = 0.0125$. The observation error is $\sigma_o \in [0.05,0.60]$. We observe all 40 degrees of freedom. We performed several assimilation runs to cover the selected ranges of parameter values, each run lasting a time interval $T = 4000$. If a filter divergence is observed, defined as a condition when the root-mean-square analysis error is larger than 3 times the observation error σ_o, then the time elapsed from the previous filter divergence is recorded; then the run is restarted by artificially repositioning the analysis near the truth. At the end of the run the average divergence time $\langle T_d \rangle$ is computed. If no divergence is observed we set $\langle T_d \rangle = 4000$. As shown in Fig. 2, in the nonlinear case it happens for some parameters values that no divergence is observed in the whole duration of the assimilation run. An example of comparison of the rms between the EKF-AUS and the EKF-AUS-NL algorithm is shown in Fig. 3 for $\tau = 0.125$ and $\sigma_o = 0.2,0.3,0.4$ and $m_l = 4$.

It is worth noticing that in Fig. 3, before the first divergence of the linear algorithm EKF-AUS, the two approaches lead practically to the same result. This is an important property of our algorithm and the consequence of not using any artificial or empirical procedure, such as covariance inflation to avoid divergence. This type of empirical procedures have as a drawback that the filter performance is reduced (i.e., the average analysis error is increased). In our approach, when nonlinear growth is actually taking place, filter divergence is avoided thanks to the nonlinear vectors that modify the estimate of the forecast error.

In order to permit a numerical comparison between the results of EKF-AUS-NL with other possible approaches, in Table II we show the rms of the analysis error averaged over the total time window of length 4000 in those cases where there is no divergence.

The results presented so far refer to the case when the number of measurements $p = n$, i.e., all state variables are observed. In most practical applications, in addition to the difficulties due to the chaoticity of the system, the observation network is largely incomplete. Therefore, we consider the case where only a small fraction of the state variables are observed every time interval. The results obtained by reducing the number of observations are presented in Fig. 4, which shows the average divergence time $\langle T_d \rangle$ for $\tau = 0.125$ and $\sigma_o = 0.10,0.15,0.20,0.25$. In detail, we report $\langle T_d \rangle$ as function of the ratio n/p, intending that we measure all the variables when $n/p = 1$, every other variable when $n/p = 2$, one over

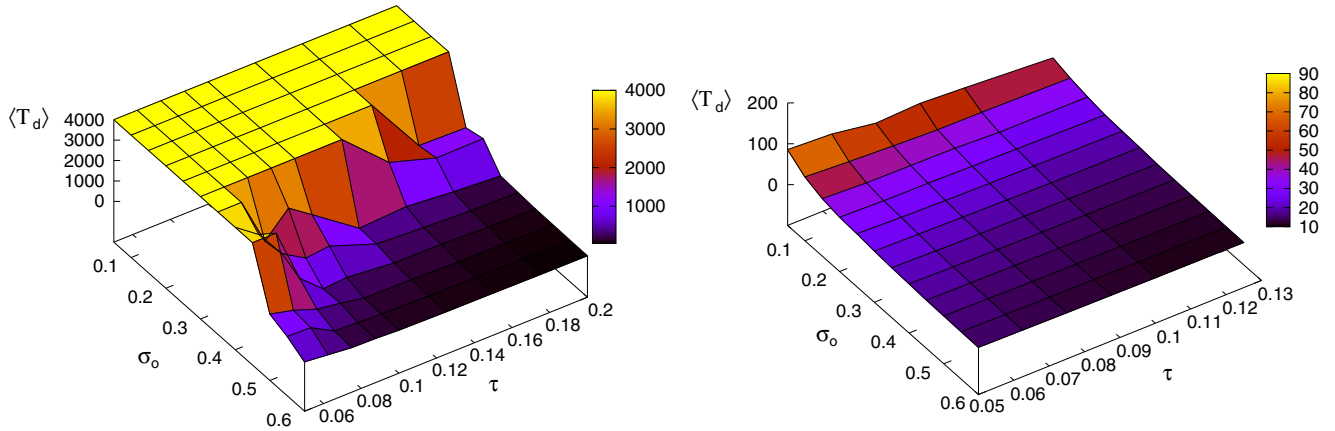

FIG. 2. (Color online) Comparison of average divergence time $\langle T_d \rangle$ as a function of time distance τ between assimilation steps and of the measurement error σ_o. Left panel: the EKF-AUS-NL algorithm with $m = 14$ and $m_l = 4$; right panel: the EKF-AUS algorithm with $m = 14$. Lighter (darker) shades indicate larger (shorter) divergence time.

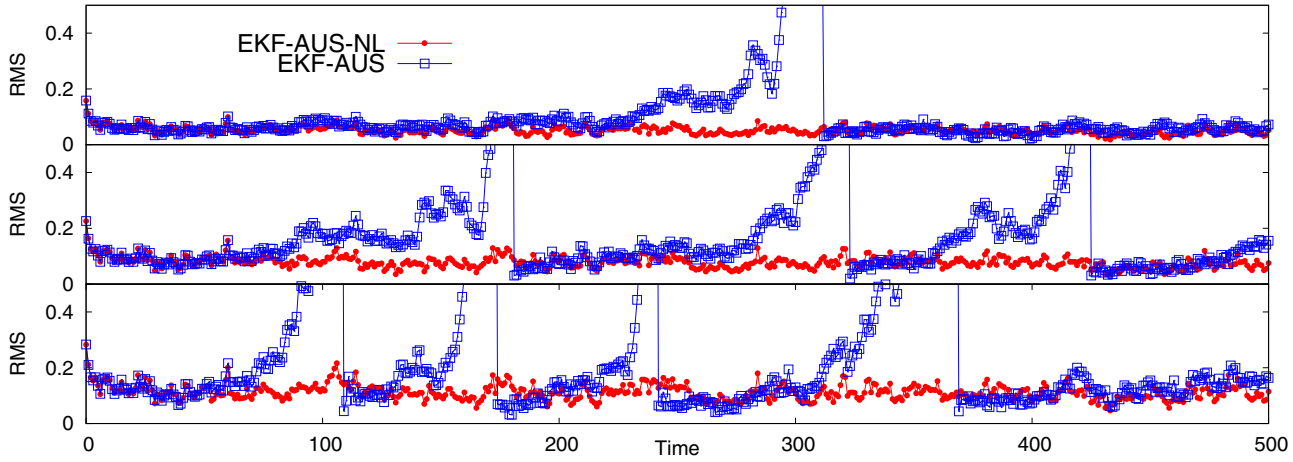

FIG. 3. (Color online) Time evolution of the rms analysis error in a sequence of 500 assimilation intervals: comparison between the EKF-AUS (blue empty square) and the EKF-AUS-NL algorithm (red filled circle) with $m_l = 4$ for $\tau = 0.125$ and $\sigma_o = 0.2,0.3,0.4$ from top to bottom. It is evident the lower rate of divergence of the nonlinear algorithm and that, before divergence, the two algorithms lead essentially to the same results.

three when $n/p = 3$, and so on. Obviously, when p decreases the divergence time also decreases because the smaller number of observed variables degrades the analysis accuracy making the system more prone to divergence. It is remarkable that even with a small number of observations ($n/p = 2,3$) no divergence occurs, showing that, provided the measurement noise and the observation interval are not too large, the EKF-AUS-NL algorithm is very effective in controlling the stability of the filter.

V. CONCLUSIONS

In this paper we have addressed the theoretical question of accounting for nonlinearities in the EKF. When error dynamics is nonlinear the use of incorrect forecast error covariance matrices deteriorates the EKF performance and it may also lead to filter divergence. Forecasting the correct PDF of the forecast error is a difficult task and empirical methods, such as covariance inflation, are often used, in operational practice, to control filter divergence, with the drawback of increasing the overall analysis error [24].

We here showed how the estimate of the forecast error can be improved by extending the EKF to account for nonlinear error dynamics. This could be done in the framework of a solution of the EKF equations that made it possible to include the nonlinearities in a rigorous way. Previous works by the authors of the present paper have in fact shown that, when the error dynamics is linear, the EKF equations can be solved within the unstable and neutral manifold of the system with an algorithm, referred to as EKF-AUS. EKF-AUS is a square-root filter implementation that uses a limited number of perturbation vectors, the Lyapunov vectors with non-negative exponents.

TABLE II. Time-averaged rms analysis error for different values of σ_o and $\tau = 0.05$ or 0.125; all the cases reported refer to runs without filter divergence ($\langle T_d \rangle = 4000$). We observe all the variables, thus $p = n$.

τ	σ_o	Averaged rms
0.05	0.05	0.00744
0.05	0.10	0.01514
0.05	0.15	0.02312
0.05	0.20	0.03137
0.05	0.25	0.04020
0.05	0.30	0.04882
0.05	0.35	0.05765
0.05	0.40	0.06783
0.05	0.45	0.07777
0.125	0.05	0.01130
0.125	0.10	0.02322
0.125	0.15	0.03579
0.125	0.20	0.04928
0.125	0.25	0.06312
0.125	0.30	0.07804

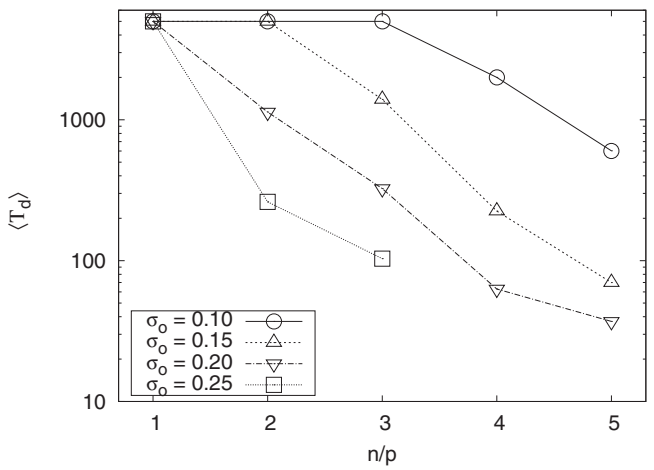

FIG. 4. Average divergence time $\langle T_d \rangle$ as a function of the ratio n/p and $\sigma_o = 0.10,0.15,0.20.0.25$. Notice that for $\sigma_o = 0.10$ and $n/p \leqslant 3$ there is still no divergence in the time interval considered (4×10^4 assimilation steps). Like in the previous figures the number of Lyapunov vectors considered for nonlinear interaction is $m_l = 4$; $n = 40$ and $\tau = 0.125$.

We here introduced nonlinear terms in the time evolution of the error: The additional directions that are a result of the interaction among the leading Lyapunov vectors are considered and used in the construction of the forecast error covariance. The important point is that with this approach we not only estimate the different magnitude of the error covariance along the unstable manifold but we are also able to evaluate in which directions the nonlinear terms are causing the error to grow. We provide an illustrative example in the Lorenz63 model, where we show that a strongly nonlinear and non-Gaussian error distribution can be dealt with by the filter by means of the leading Lyapunov vector and one nonlinear vector. Compared with previous studies performed with the same system that involved huge numbers of ensemble members [24] or onerous computations [21] this is a substantial improvement.

We then tested the performance of the method in the Lorenz96 model showing the great improvement obtained in a wide range of parameter values where the nonlinear EKF-AUS-NL can prevent divergence when the EKF fails to do so. Besides its theoretical interest, this method constitutes an improvement in terms of computational efficiency. In fact, as shown in Appendix B, even when the tangent linear and second-order perturbation equations are not available, the nonlinear terms can be easily computed by breeding with linear and nonlinear renormalization amplitudes. The results we presented are important in practical implementations: The possibility to take into account the nonlinear evolution of the forecast error presented in this paper can be extended to other data assimilation schemes, such as EnKFs or 4DVar, used in operational forecasting models.

ACKNOWLEDGMENTS

L.P. thanks SSD-PESCA and RITMARE Research Projects (MIUR–Italian Research Ministry).

APPENDIX A

Before showing the detailed calculations of the nonlinear terms in the error evolution we briefly review the main idea behind the square-root implementation of the Kalman filter. The main idea is to parametrize the matrices $\mathbf{P}^a$ and $\mathbf{P}^f$. Indicating with $\mathbf{P}$ the generic covariance matrix, we define its square root $\mathbf{X}$ with the condition

$$\mathbf{P} = \mathbf{X}\mathbf{X}^T. \tag{A1}$$

We notice that the square root $\mathbf{X}$ is not uniquely defined. In Ref. [13] and in this paper we have chosen $\mathbf{X}$ to be a set of orthogonalized vectors. All the formalism of Sec. II describes the time evolution of the columns of $\mathbf{X}$, called "perturbations," that were shown in Ref. [13] to asymptotically span the same space as the Lyapunov vectors with non-negative exponents.

The correspondence between the columns or perturbations and the covariance matrix $\mathbf{P}$ can be written in two ways. The perturbations can be interpreted as the columns of $\mathbf{P}$. For example, with two perturbations $\mathbf{v}_1, \mathbf{v}_2$ we have

$$\mathbf{P} = \mathbf{X}\mathbf{X}^T = (\mathbf{v}_1 \mathbf{v}_2)\left(\mathbf{v}_1^T \mathbf{v}_2^T\right). \tag{A2}$$

Going to the index representation and using the Einstein's notation we have

$$\begin{aligned} P_{ij} &= X_{ik} X_{jk} = v_i^s v_j^s = \sum_s v_i^s v_j^s \\ &= \sum_s \int dt f_i^s(\mathbf{v}^s, \mathbf{v}^t, \ldots) \int dt' f_j^s(\mathbf{v}^s, \mathbf{v}^t, \ldots), \end{aligned} \tag{A3}$$

where the vectors $\mathbf{v}^s$ obey a differential equation of the form

$$\frac{dv_i^s}{dt} = f_i^s(\mathbf{v}^s, \mathbf{v}^t, \ldots). \tag{A4}$$

We are now ready to calculate the different terms of Eq. (23).

Let us start from the mixed term $\langle \mathcal{N}_i \mathcal{L}_j \rangle$. We obtain

$$\begin{aligned} \langle \mathcal{N}_i \mathcal{L}_j \rangle &= \left\langle \Delta_j(0) \int_0^\tau \frac{1}{2} F_{i;jk} \sum_{s=1}^m \alpha_s \mathbf{X}_{js}^a \sum_{r=1}^m \alpha_r \mathbf{X}_{kr}^a \right\rangle \\ &+ \left\langle \int_0^\tau dt' F_{j,k} \sum_{s=1}^m \alpha_s \mathbf{X}_{ks}^a \int_0^\tau \frac{1}{2} F_{i;jk} \right. \\ &\left. \times \sum_{s=1}^m \alpha_s \mathbf{X}_{js}^a \sum_{r=1}^m \alpha_r \mathbf{X}_{kr}^a \right\rangle. \end{aligned} \tag{A5}$$

The second term is zero, thanks to the hypothesis that the α are Gaussian and the third moment of a Gaussian variable is null. The first term becomes, using that $\langle \alpha_s \alpha_r \rangle = \delta_{sr}$,

$$\begin{aligned} \langle \mathcal{N}_i \mathcal{L}_j \rangle &= \Delta_j(0) \int_0^\tau \frac{1}{2} F_{i;jk} \sum_{s=1}^m \mathbf{X}_{js}^a \mathbf{X}_{ks}^a \\ &= \Delta_j(0) \int_0^\tau dt' \mathcal{D}_i(t'). \end{aligned} \tag{A6}$$

Here and in the following we use the notation

$$\mathcal{C}_{i,sr} \equiv \frac{1}{2} F_{i;lk} \mathbf{X}_{ls}^a \mathbf{X}_{kr}^a, \quad \mathcal{D}_i \equiv \frac{1}{2} F_{i;lk} \sum_{s=1}^m \mathbf{X}_{ls}^a \mathbf{X}_{ks}^a = \sum_{s=1}^m \mathcal{C}_{i,ss}. \tag{A7}$$

Let us calculate the term $\langle \mathcal{N}_i \mathcal{N}_j \rangle$. We have

$$\begin{aligned} \langle \mathcal{N}_i \mathcal{N}_j \rangle &= \frac{1}{4} \int_0^\tau dt' \int_0^\tau dt'' F_{i;lk} F_{j;np} \sum_{s_1=1}^m \sum_{t_1=1}^m \sum_{s_2=1}^m \\ &\times \sum_{t_2=1}^m \mathbf{X}_{ls_1}^a \mathbf{X}_{kt_1}^a \mathbf{X}_{ns_2}^a \mathbf{X}_{pt_2}^a \langle \alpha_{s_1} \alpha_{t_1} \alpha_{s_2} \alpha_{t_2} \rangle. \end{aligned} \tag{A8}$$

If the error distribution at time t is approximately Gaussian, α_i are with zero mean and unitary variance. Notice that α_i are constant in time while the column vectors of $\mathbf{X}^a$ evolve to become those of $\mathbf{X}^f$. Noticing that

$$\sum_{s_1=1}^m \sum_{t_1=1}^m \sum_{s_2=1}^m \sum_{t_2=1}^m \mathbf{X}_{ls_1}^a \mathbf{X}_{kt_1}^a \mathbf{X}_{ns_2}^a \mathbf{X}_{pt_2}^a \langle \alpha_{s_1} \alpha_{t_1} \alpha_{s_2} \alpha_{t_2} \rangle = \sum_{s=1}^m \sum_{r=1}^m \mathbf{X}_{ls}^a \mathbf{X}_{ks}^a \mathbf{X}_{nr}^a \mathbf{X}_{pr}^a + \sum_{s=1}^m \sum_{r=1}^m \mathbf{X}_{ls}^a \mathbf{X}_{ns}^a \mathbf{X}_{kr}^a \mathbf{X}_{pr}^a + \sum_{s=1}^m \sum_{r=1}^m \mathbf{X}_{ls}^a \mathbf{X}_{ps}^a \mathbf{X}_{kr}^a \mathbf{X}_{nr}^a, \tag{A9}$$

and using the property that $F_{i;np} = F_{i;pn}$, we have

$$\begin{aligned}\langle \mathcal{N}_i \mathcal{N}_j \rangle &= \int_0^\tau dt' \int_0^\tau dt'' \left\{ F_{i;lk} \sum_{s=1}^{m} \mathbf{X}^a_{ls} \mathbf{X}^a_{ks} F_{j;np} \sum_{r=1}^{m} \mathbf{X}^a_{nr} \mathbf{X}^a_{pr} + 2 F_{i;lk} F_{j;np} \sum_{s=1}^{m} \sum_{r=1}^{m} \mathbf{X}^a_{ls} \mathbf{X}^a_{ns} \mathbf{X}^a_{kr} \mathbf{X}^a_{pr} \right\} \\ &= \int_0^\tau dt' \int_0^\tau dt'' \left\{ \mathcal{D}_i \mathcal{D}_j + 2 \sum_{s=1}^{m} \sum_{r=1}^{m} \mathcal{C}_{i,sr} \mathcal{C}_{j,sr} \right\} = \int_0^\tau dt' \int_0^\tau dt'' \left\{ 3\mathcal{D}_i \mathcal{D}_j + 2 \sum_{s=1}^{m} \sum_{r=1, r\neq s}^{m} \mathcal{C}_{i,sr} \mathcal{C}_{j,sr} \right\} \\ &= \int_0^\tau dt \sqrt{3} \mathcal{D}_i \int_0^\tau \sqrt{3} dt \mathcal{D}_j + \sum_{s=1}^{m} \sum_{r=1, r\neq s}^{m} \int_0^\tau \sqrt{2} \mathcal{C}_{i,sr} \int_0^\tau \sqrt{2} \mathcal{C}_{j,sr}. \end{aligned} \tag{A10}$$

We can now write down the complete form of the $\mathbf{P}^f$. Remembering that the product $\langle \mathcal{L}_i \mathcal{L}_j \rangle$ is the linear evolution given by Eq. (7) we obtain

$$\mathbf{P}^f = \mathbf{M}\mathbf{X}_a (\mathbf{M}\mathbf{X}_a)^T + \Delta_j(0) \int_0^\tau dt' \mathcal{D}_i(t') + \int_0^\tau dt \sqrt{3} \mathcal{D}_i \int_0^\tau \sqrt{3} dt' \mathcal{D}_j + \sum_{s=1}^{m} \sum_{r=1, r\neq s}^{m} \int_0^\tau dt \sqrt{2} \mathcal{C}_{i,sr} \int_0^\tau dt' \sqrt{2} \mathcal{C}_{j,sr}. \tag{A11}$$

Up to this point the calculations have been exact. To perform the assimilation to preserve the square-root structure of the filter we decided to neglect the second term. Indeed, this term is the only one that cannot easily be arranged as a factorized term, i.e., in term of a square root.

Moreover, we want to stress that when the importance of the nonlinear terms in avoiding filter divergence is more relevant, then the relative contribution of the analysis error at time $t = 0$, $\Delta(0)$ is negligible with respect to the error terms that are growing due to the nonlinear time evolution.

All the other terms are exactly in the form given by Eq. (A3), so we may easily write down the differential equation driving the time evolution of all the columns of the covariance matrix from $\mathbf{P}^a$ to $\mathbf{P}^f$ as

$$\begin{aligned} \frac{d}{dt}\mathbf{X}_{is} &= F_{i,j}\mathbf{X}_{js} \quad s \leqslant m, \\ \frac{d}{dt}\mathbf{X}_{im+1} &= F_{i,j}\mathbf{X}_{jm+1} + \frac{\sqrt{3}}{2} F_{i;lk} \sum_{r=1}^{m} \mathbf{X}^a_{lr} \mathbf{X}^a_{kr}, \\ \frac{d}{dt}\mathbf{X}_{im+1+r} &= F_{i,j}\mathbf{X}_{jm+1+s} + \frac{\sqrt{2}}{2} F_{i;lk} \mathbf{X}^a_{lr} \mathbf{X}^a_{kq}, \end{aligned} \tag{A12}$$

where $r,q \in [1,m]$ with $r < q$ (to avoid to repeat the $r = q$ case) while s in the last equation increases of a unit for each different couple of indexes p,q. This means that each couple of index r,q leads to a separate vector of index $m + 1 + s$.

We must stress now that the exact division in terms of $\mathcal{D}_i$ and cross-term $\mathcal{C}_{i,rq}$ together with the precise prefactors $\sqrt{3}$ or $\sqrt{2}$ in front of each term strongly depends on the Gaussian assumption. For a practical implementation we decided to put a constant prefactor $\bar{\alpha}$ in front of all the nonlinear terms. Moreover, as discussed in the text, the main effect of the nonlinear terms is to take into account all the new directions in the phase-space along which the error is distributed. From a theoretical point of view, to keep the terms $\mathcal{C}_{i,rr}$ together with the term $\mathcal{D}_i$ or separated is equivalent, as all the vectors are processed with the Graham-Schmidt algorithm in Eq. (8). This corresponds to the fact the the square root of a symmetric matrix is not unique.

For this reason, to keep the span of the nonlinear vectors as "large" as possible from a numerical point of view, we decided to consider all the vectors driven by the terms $\mathcal{C}_{i,rq}$ (also when $r = q$) separated considering all the nonlinear interactions for the first (largest) m_l linear vectors. Also, the prefactor $\sqrt{3}$ or $\sqrt{2}$, which deeply depends on the Gaussian assumption, is substituted with a fixed factor $\bar{\alpha}$ equal for all the nonlinear vectors. After these changes we obtain the Eq. (25) used in this paper.

APPENDIX B

Very often it can happen that the differential equation

$$\frac{d\mathbf{x}}{dt} = F(\mathbf{x}) \tag{B1}$$

that drives the dynamical system is known but there are difficulties to define or calculate the first and second derivative of $F(\mathbf{x})$. In this appendix we generalize our method to this case.

As a first step we have to find a typical scale η (in the phase space, not in the physical space of the model) at which the evolution of the difference between two trajectories is essentially linear. There are different techniques to estimate η and we refer the reader to the literature like, for example, Refs. [33,34].

As in the standard case we have a trajectory that defines the analysis $\mathbf{x}^a(0)$. The nonlinear operator driving the trajectory from the analysis time $t = 0$ to the forecast time $t = \tau$ is called $\mathcal{M}(\mathbf{x}^a)$. We thus have

$$\mathbf{x}^f(\tau) = \mathcal{M}[\mathbf{x}^a(0)]. \tag{B2}$$

Given at time $t = 0$ the $m + m_l(m_l + 1)/2$ perturbations $\mathbf{X}^a$, let us define the k-th column of $\mathbf{X}^a$ as $\delta\mathbf{x}^a_k$. We obtain the first m trajectories in this way:

$$\mathbf{x}_k(0) = \mathbf{x}^a(0) + \eta \frac{\delta\mathbf{x}^a_k}{\|\delta\mathbf{x}^a_k\|}, \quad k \in [1,m], \tag{B3}$$

and then the remaining $m_l(m_l+1)/2$ trajectories are obtained as

$$\mathbf{x}_s(0) = \mathbf{x}^a(0) + \frac{1}{2}\left[\delta\mathbf{x}^a_r + \delta\mathbf{x}^a_q\right],$$
$$r,q \in [1,m_l],\ q \leqslant r; s(q,r) = m + \sum_{r=1}^{m_l}\sum_{q=1}^{q\leqslant r} 1. \quad \text{(B4)}$$

At this point all the trajectories are evolved up to time $t=\tau$ using the full nonlinear system:

$$\mathbf{x}_k(\tau) = \mathcal{M}(\mathbf{x}_k(0)), \quad k \in [1,m+m_l(m_l+1)/2]. \quad \text{(B5)}$$

To obtain the perturbations $\mathbf{X}^f$ to be inserted in Eq. (8) we proceed as follows. For the first m vectors,

$$\delta\mathbf{x}^f_k(\tau) = \frac{\left\|\delta\mathbf{x}^a_k(0)\right\|}{\eta}[\mathbf{x}_k(\tau) - \mathbf{x}^f(\tau)], \quad k \in [1,m], \quad \text{(B6)}$$

while for the remaining columns we have

$$\delta\mathbf{x}^f_s(\tau) = \bar{\alpha}\left\{\mathbf{x}_s(\tau) - \mathbf{x}^f(\tau) - \frac{1}{2}\left[\delta\mathbf{x}^f_r(\tau) + \delta\mathbf{x}^f_q(\tau)\right]\right\},$$
$$r,q \in [1,m_l],\ q \leqslant r; s(q,r) = m + \sum_{r=1}^{m_l}\sum_{q=1}^{q\leqslant r} 1, \quad \text{(B7)}$$

where $\delta\mathbf{x}^f_r(\tau), \delta\mathbf{x}^f_q(\tau)$ are given by Eq. (B6), being $r,q < m$. The meaning of the last equation is simply to assign to the nonlinear perturbations the difference between the linear (the terms inside the square brackets) and the nonlinear time evolution, multiplied by the factor $\bar{\alpha}$. After these steps the algorithm restarts from Eq. (8).

[1] A. H. Jazwinski, *Stochastic Processes and Filtering Theory* (Academic Press, New York, 1970).
[2] M. S. Grewal, L. R. Weill, and A. P. Andrews, *Global Positioning Systems, Inertial Navigation and Integration* (John Wiley & Sons, New York, 2007).
[3] P. de Rosnay, M. Drusch, D. Vasiljevic, G. Balsamo, C. Albergel, and L. Isaksen, Q. J. Roy. Meteorol. Soc. **139**, 1199 (2013).
[4] A. Duerinckx, R. Hamdi, J. F. Mahfouf, and P. Termonia, Geosci. Model Dev. Discuss. **7**, 7151 (2014).
[5] S. S. Haykin (ed.), *Kalman Filtering and Neural Networks* (Wiley, New York, 2001).
[6] I. A. Essa and A. P. Pentland, IEEE T. Pattern Anal. **19**, 757 (1997).
[7] M. Charkhgard and M. Farrokhi, IEEE T. Ind. Electron. **57**, 4178 (2010).
[8] C. Hu, B. D. Youn, and J. Chung, Appl. Energ. **92**, 694 (2012).
[9] V. P. Oikonomou, A. T. Tzallas, S. Konitsiotis, D. G. Tsalikakis, and D. I. Fotiadis, in *The Use of Kalman Filter in Biomedical Signal Processing, Kalman Filter Recent Advances and Applications*, edited by V. M. Moreno and A. Pigazo (InTech, Vienna, 2009).
[10] T. Oakes, L. Tang, R. G. Landers, and S. N. Balakrishnan, in *Kalman Filtering for Manufacturing Processes, Kalman Filter Recent Advances and Applications*, edited by V. M. Moreno and A. Pigazo (InTech, Vienna, 2009).
[11] V. M. Moreno and A. Pigazo (eds.), *Kalman Filter Recent Advances and Applications* (InTech, Vienna, 2009).
[12] C. Sammut and G. I. Webb (eds.), *Encyclopedia of Machine Learning* (Springer Science & Business Media, Berlin, 2011).
[13] A. Trevisan and L. Palatella, Nonlin. Processes Geophys. **18**, 243 (2011).
[14] C. L. Thornton and G. J. Bierman, NASA Technical Report No. NASA-CR-148278, 1976.
[15] A. Carrassi, A. Trevisan, and F. Uboldi, Tellus **59**, 101 (2007).
[16] F. Uboldi and A. Trevisan, Nonlin. Processes Geophys. **13**, 67 (2006).
[17] A. Trevisan and F. Uboldi, J. Atmos. Sci. **61**, 103 (2004).
[18] A. Carrassi, M. Ghil, A. Trevisan, and F. Uboldi, Chaos **18**, 023112 (2008).
[19] A. Carrassi, A. Trevisan, L. Descamps, O. Talagrand, and F. Uboldi, Nonlin. Proc. Geophys. **15**, 503 (2008).
[20] E. N. Lorenz, *Predictability: A Problem Partly Solved, Proc. Seminar on Predictability* (European Center for Medium-Range Weather Forecasting, Shinfield Park, Reading, UK, 1996), p. 1.
[21] R. N. Miller, M. Ghil, and F. Gauthier, J. Atmos. Sci. **51**, 1037 (1994).
[22] E. Kalnay, *Atmospheric Modeling, Data Assimilation, and Predictability* (Cambridge University Press, Cambridge, UK, 2003).
[23] G. Evensen, J. Geophys. Res. **99**, 10143 (1994).
[24] G. Evensen, Ocean Dyn. **53**, 343 (2003).
[25] E. Ott, B. R. Hunt, I. Szunyogh, A. V. Zimin, E. J. Kostelich, M. Corazza, E. Kalnay, D. J. Patil, and J. A. Yorke, Tellus A **56**, 415 (2004).
[26] M. Bocquet, Nonlin. Processes Geophys. **18**, 735 (2011).
[27] G.-H. Crystal Ng, D. McLaughlin, D. Entekhabi, and A. Ahanin, Tellus A **63**, 958 (2011).
[28] A. Trevisan, M. D'Isidoro, and O. Talagrand, Q. J. Roy. Meteorol. Soc. **136**, 487 (2010).
[29] F. X. Le Dimet and O. Talagrand, Tellus A **38**, 97 (1986).
[30] O. Talagrand and P. Courtier, Q. J. Roy. Meteorol. Soc. **113**, 1311 (1987).
[31] E. N. Lorenz, J. Atmos. Sci. **20**, 130 (1963).
[32] G. Benettin, L. Galgani, A. Giorgilli, and J. M. Strelcyn, Meccanica **15**, 9 (1980).
[33] Z. Toth and E. Kalnay, Bull. Am. Met. Soc. **74**, 2317 (1993).
[34] Z. Toth and E. Kalnay, Mon. Weather Rev. **125**, 3297 (1997).